LETTERS
PUBLISHED ONLINE: 19 SEPTEMBER 2016 | DOI: 10.1038/NPHOTON.2016.180
nature photonics

Quantum teleportation across a metropolitan fibre network

Raju Valivarthi[1†], Marcel.li Grimau Puigibert[1†], Qiang Zhou[1†], Gabriel H. Aguilar[1†], Varun B. Verma[2], Francesco Marsili[3], Matthew D. Shaw[3], Sae Woo Nam[2], Daniel Oblak[1] and Wolfgang Tittel[1*]

If a photon interacts with a member of an entangled photon pair via a Bell-state measurement (BSM), its state is teleported over principally arbitrary distances onto the pair's second member[1]. Since 1997, this puzzling prediction of quantum mechanics has been demonstrated many times[2]. However, with two exceptions[3,4], only the photon that received the teleported state, if any, travelled far, while the photons partaking in the BSM were always measured close to where they were created. Here, using the Calgary fibre network, we report quantum teleportation from a telecom photon at 1,532 nm wavelength, interacting with another telecom photon after both have travelled several kilometres and over a combined beeline distance of 8.2 km, onto a photon at 795 nm wavelength. This improves the distance over which teleportation takes place to 6.2 km. Our demonstration establishes an important requirement for quantum repeater-based communications[5] and constitutes a milestone towards a global quantum internet[6].

Although the possibility to teleport quantum states, including the teleportation of entangled states, has been verified many times using different physical systems (see ref. 2 for a recent review), the maximum distance over which teleportation is possible (which we define to be the spatial separation between the BSM and the photon, at the time of this measurement, that receives the teleported state) has so far received virtually no experimental attention. (See Supplementary Section 2 for a motivation for this arguably most natural definition and for a description of various experiments in this regard.) To date, only two experiments have been conducted in a setting that resulted in a teleportation distance exceeding the laboratory scale[3,4], even if in a few demonstrations the beeline distance travelled by the photon that receives the teleported state has been much longer[7,8].

The reason for stressing the importance of distance is linked to the ability to exploit teleportation in various quantum information applications. One important example is the task of extending quantum communication distances using quantum repeaters[5], most of which rely on the creation of light–matter entanglement, for example, by creating an entangled two-photon state out of which one photon is absorbed by a quantum memory for light[9] and entanglement swapping[10]. The latter has in common the BSM with standard teleportation, but the photon carrying the state to be teleported is itself a member of an entangled pair. Entanglement swapping is therefore sometimes referred to as teleportation of entanglement. To be useful in such a repeater, two entangled photon pairs must be created far apart, and the BSM, which heralds the existence of the two partaking photons and hence of the remaining members of the two pairs, should, for optimal performance, take place approximately halfway between these two locations.

Yet, due to the difficulty in guaranteeing the indistinguishability of the two interacting photons after their transmission through long and noisy quantum channels[11], entanglement swapping or standard teleportation in the important midpoint configuration has only been reported very recently outside the laboratory[4]. This work exploited the heralding nature of the BSM for the first loophole-free violation of a Bell inequality—a landmark result that exemplifies the importance of this configuration. However, the two photons featured a wavelength of ~637 nm, which, due to high loss during transmission through optical fibre, makes it impossible to extend the transmission distance to tens, let alone hundreds, of kilometres. In all other demonstrations, either the travel distances of the two photons were small, or they were artificially increased using fibre on spool[3,12–15], effectively increasing the travel time and transmission loss, and hence decreasing communication rates, rather than real separation. Here, we report the first demonstration of quantum teleportation over several kilometres in the mid-point configuration and with photons at telecommunication wavelength.

An aerial map of Calgary, identifying the locations of Alice, Bob and Charlie, is shown in Figs 1 and 2. These depict the schematics of the experimental set-up. Alice, located in Manchester (a Calgary neighbourhood), prepares phase-randomized attenuated laser pulses at 1,532 nm wavelength with different mean photon numbers $\mu_A \ll 1$ in various time-bin qubit states $|\psi\rangle_A = \alpha|e\rangle + \beta e^{i\phi}|\ell\rangle$, where $|e\rangle$ and $|\ell\rangle$ denote early and late temporal modes, respectively, ϕ is a phase factor, and α and β are real numbers that satisfy $\alpha^2 + \beta^2 = 1$. Using 6.2 km of deployed fibre, she sends her qubits to Charlie, who is located 2.0 km away in a building next to Calgary City Hall. Bob, located at the University of Calgary, 6.2 km from Charlie, creates pairs of photons—one at 1,532 nm and one at 795 nm—in the maximally time-bin entangled state $|\phi^+\rangle = 2^{-1/2}(|e,e\rangle + |\ell,\ell\rangle)$. He sends the telecommunication-wavelength photons through 11.1 km of deployed fibre to Charlie, where they are probabilistically projected jointly with the photons from Alice onto the maximally entangled state $|\psi^-\rangle = 2^{-1/2}(|e,\ell\rangle - |\ell,e\rangle)$. As we show in the Supplementary Information, this leads to the 795 nm wavelength photon at Bob acquiring the state $|\psi\rangle_B = \sigma_y|\psi\rangle_A$, where σ_y is the Pauli operator describing a bit-flip combined with a phase-flip. In other words, Charlie's measurement results in the teleportation of Alice's photon's state, modulo a unitary transformation, over 6.2 km distance onto Bob's 795 nm wavelength photon.

To confirm successful quantum teleportation, Bob then performs a variety of projective measurements on this photon, the outcomes of which, conditioned on a successful BSM at Charlie, are analysed using different approaches (see Methods for more information on

[1]Institute for Quantum Science and Technology, and Department of Physics & Astronomy, University of Calgary, 2500 University Drive NW, Calgary, Alberta T2N 1N4, Canada. [2]National Institute of Standards and Technology, Boulder, Colorado 80305, USA. [3]Jet Propulsion Laboratory, California Institute of Technology, 4800 Oak Grove Drive, Pasadena, California 91109, USA. †These authors contributed equally to this work. *e-mail: wtittel@ucalgary.ca

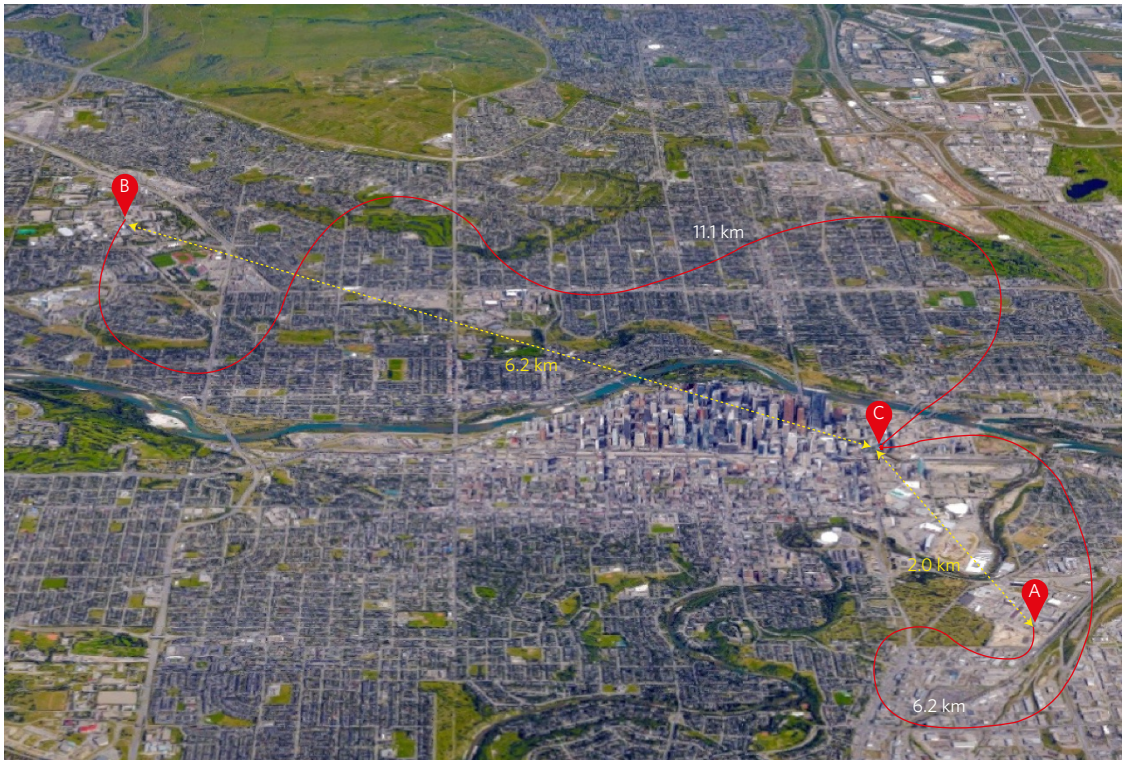

Figure 1 | Aerial view of Calgary. Alice 'A' is located in Manchester, Bob 'B' at the University of Calgary and Charlie 'C' in a building next to City Hall in Calgary downtown. The teleportation distance—in our case the distance between Charlie and Bob—is 6.2 km. All fibres belong to the Calgary telecommunication network but, during the experiment, they only carry signals created by Alice, Bob or Charlie and were otherwise 'dark'. Imagery ©2016 Google. Map data ©2016 Google.

how data are taken). We point out that the 795 nm wavelength photons are measured before the BSM, thus realizing a scenario where teleportation is achieved *a posteriori*[16,17].

The main difficulty in long-distance quantum teleportation is to ensure the required indistinguishability (in spectral, temporal, spatial and polarization degrees of freedom) between the two photons subjected to the BSM at Charlie (in our case the photons are only 70 ps long), despite them being created by independent sources and having travelled over several kilometres of deployed fibre. As we show in Fig. 3, varying environmental conditions during the measurements significantly impact the polarization and arrival times of the photons. Thus, quantum teleportation is only possible with active and automated stabilization of the polarization and of the path-length difference. For the former we employ a polarization tracker and for the latter we use a novel approach based on Hong–Ou–Mandel (HOM) quantum interference (see Methods and Supplementary Section 3 for details).

To verify successful teleportation, first, Alice creates photons in an equal superposition of $|e\rangle$ and $|\ell\rangle$ with a fixed phase, and Bob makes projection measurements onto states described by such superpositions with various phases. Conditioned on a successful BSM at Charlie, we find sinusoidally varying triple-coincidence count rates with a visibility of $(38 \pm 4)\%$ and an average of 17.0 counts per minute. This result alone already represents a strong indication of quantum teleportation: assuming that the teleported state is a statistical mixture of a pure state and white noise, the visibility consistent with the best classical strategy and assuming Alice creates single photons is 1/3 (ref. 18). However, here we use this result merely to establish absolute phase references for Alice's and Bob's interferometers (Supplementary Section 4).

Being able to control the absolute phase values, we can now create photons in, and project them onto, well-defined states, for example, $|e\rangle$, $|\ell\rangle$, $|\pm\rangle \equiv 2^{-1/2}(|e\rangle \pm |\ell\rangle)$ and $|\pm i\rangle \equiv 2^{-1/2}(|e\rangle \pm i|\ell\rangle)$. This allows us to reconstruct the density matrices ρ_{out} of various quantum states after teleportation and, in turn, calculate the fidelities $F = {}_{\mathrm{B}}\langle\psi|\rho_{\mathrm{out}}|\psi\rangle_{\mathrm{B}}$ with the expected states $|\psi\rangle_{\mathrm{B}}$. The results, depicted in Figs 4 and 5, show that the fidelity for all four prepared states exceeds the maximum classical value of 2/3 (ref. 18). In particular, the average fidelity $\langle F\rangle = [F_e + F_l + 2(F_+ + F_{+i})]/6 = (78 \pm 1)\%$ violates this threshold by 12 standard deviations.

One may conclude that this result shows the quantum nature of the disembodied state transfer between Charlie and Bob. However, strictly speaking, the 2/3 bound only applies to Alice's state being encoded into a single photon, while our demonstration, as others before, relied on attenuated laser pulses. To extract the appropriate experimental value, we therefore take advantage of the so-called decoy-state method, which was developed for quantum key distribution (QKD) to assess an upper bound on the error rate introduced by an eavesdropper on single photons emitted by Alice[19,20]. Here, we instead use it to characterize how a quantum channel—in our case the concatenation of the direct transmission from Alice to Charlie and the teleportation from Charlie to Bob—impacts on the teleportation fidelity of quantum states encoded into individual photons[21]. Towards this end, we vary the mean number of photons per qubit emitted at Alice between three optimized values, $\mu_{\mathrm{A}} \in \{0,\ 0.014,\ 0.028\}$ and measure error rates and transmission probabilities for each value independently (see Supplementary Section 6 for details of how to extract the single-photon fidelity from these measurements). The results, also depicted in Fig. 5, show again that the fidelities for all tested states exceed the maximum value of 2/3 achievable in classical teleportation. We note the good agreement between the measured values and those predicted by our model (described in Supplementary Section 5), which takes into account various independently characterized system imperfections (no fit). This allows us to identify that deviations of the measured fidelities from unity (that is, from ideal teleportation) are mostly due to the

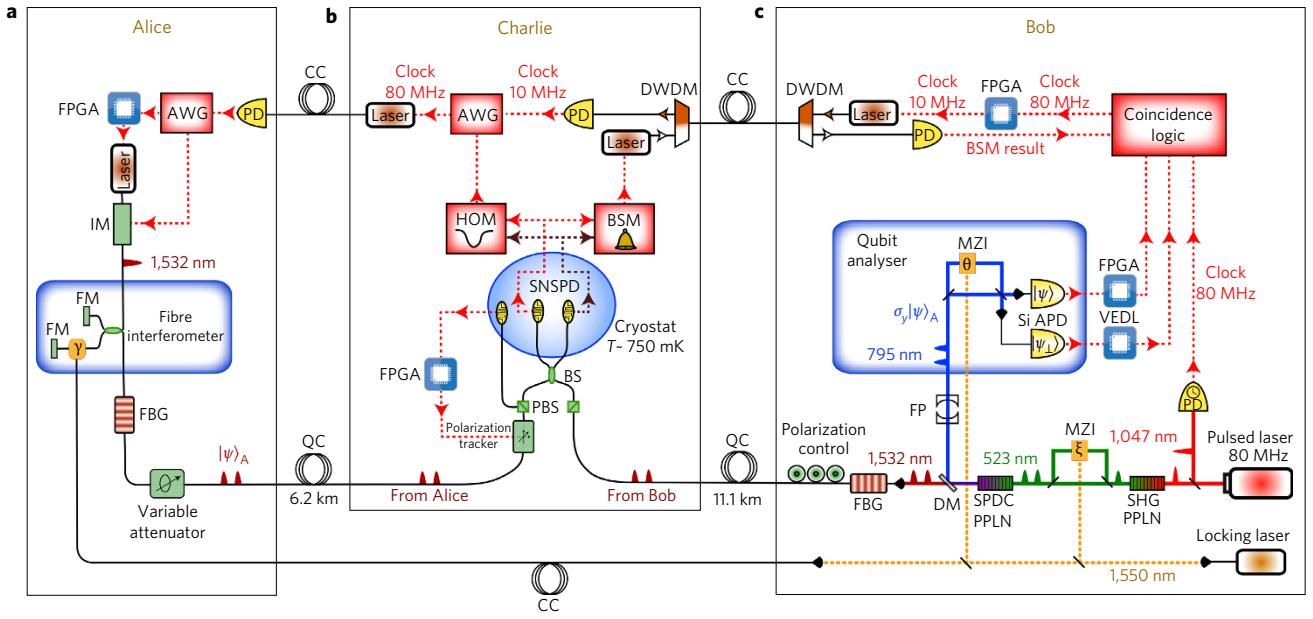

Figure 2 | Schematics of the experimental set-up. a, Alice's set-up. An intensity modulator (IM) tailors 20-ps-long pulses of light at an 80 MHz rate out of 10-ns-long, phase-randomized laser pulses at 1,532 nm wavelength. Subsequently, a widely unbalanced fibre interferometer with Faraday mirrors (FMs), active phase control (see Methods) and path-length difference equivalent to 1.4 ns travel time difference creates pulses in two temporal modes or bins. Following their spectral narrowing by means of a 6-GHz-wide fibre Bragg grating (FBG) and attenuation to the single-photon level, the time-bin qubits are sent to Charlie via a deployed fibre—referred to as a quantum channel (QC)—featuring 6 dB loss. **b**, Bob's set-up. Laser pulses at 1,047 nm wavelength and 6 ps duration from a mode-locked laser are frequency-doubled (SHG) in a periodically poled lithium-niobate (PPLN) crystal and passed through an actively phase-controlled Mach–Zehnder interferometer (MZI) that introduces the same 1.4 ns delay as between Alice's time-bin qubits. Spontaneous parametric downconversion (SPDC) in another PPLN crystal and pump rejection using an interference filter (not shown) results in the creation of time-bin entangled photon pairs[28] at 795 and 1,532 nm wavelength with mean probability μ_{SPDC} up to 0.06. The 795 nm and 1,532 nm (telecommunication-wavelength) photons are separated using a dichroic mirror (DM) and subsequently filtered to 6 GHz by a Fabry–Perot (FP) cavity and an FBG, respectively. The telecom photons are sent through deployed fibre featuring 5.7 dB loss to Charlie, and the state of the 795 nm wavelength photons is analysed using another interferometer (again introducing a phase-controlled travel-time difference of 1.4 ns) and two single-photon detectors based on silicon avalanche photodiodes (Si-APD) with 65% detection efficiency. **c**, Charlie's set-up. A beamsplitter (BS) and two WSi superconducting nanowire single-photon detectors[29] (SNSPD), cooled to 750 mK in a closed-cycle cryostat and with 70% system detection efficiency, allow the projection of biphoton states (one from Alice and one from Bob) onto the $|\psi^-\rangle$ Bell state. To ensure indistinguishability of the two photons at the BSM, we actively stabilize the photon arrival times and polarization, the latter involving a polarization tracker and polarizing beamsplitters (PBSs), as explained in the Methods. Various synchronization tasks are performed through deployed fibres, referred to as classical channels (CC) and aided by dense-wavelength division multiplexers (DWDM), photodiodes (PDs), arbitrary waveform generators (AWGs) and field-programmable gate arrays (FPGAs) (for details see Methods).

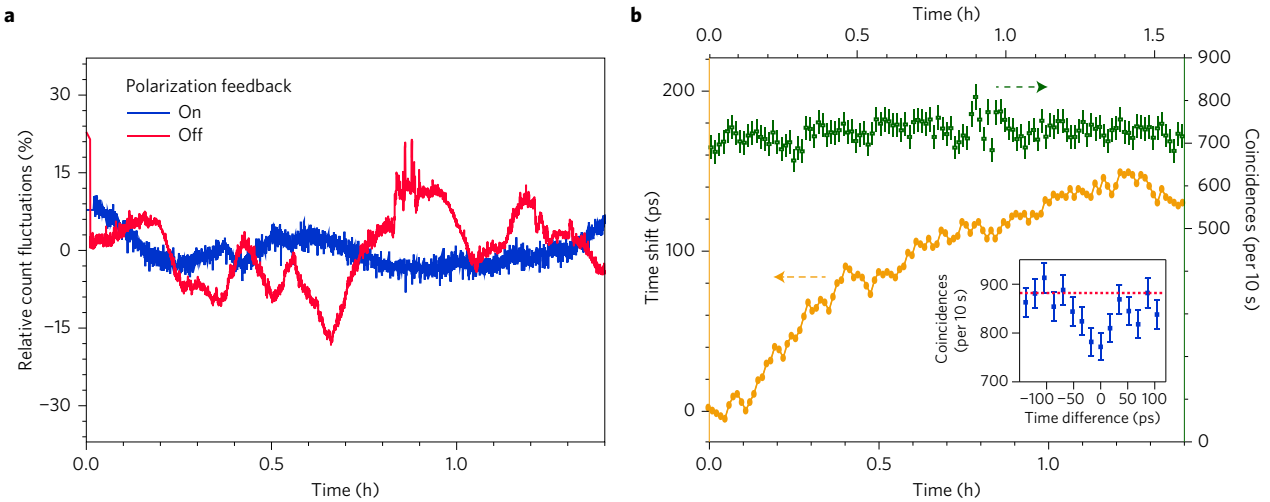

Figure 3 | Indistinguishability of photons at Charlie. a, Fluctuations of the count rate of a single SNSPD at the output of Charlie's BS with and without polarization feedback. **b**, Orange filled circles: the change in the generation time of Alice's qubits that is applied to ensure they arrive at Charlie's BSM at the same time as Bob. Green open squares: coincidence counts per 10 s with timing feedback engaged, showing locking to the minimum of the HOM dip (see Methods and Supplementary Section 3 for details). Inset: rate of coincidences between counts from SNSPDs as a function of arrival time difference, displaying a HOM dip[30] when photon-arrival times at the BS are equal. The dashed red line shows the coincidence rate in the case of completely distinguishable photons. All error bars (one standard deviation) are calculated assuming Poissonian detection statistics.

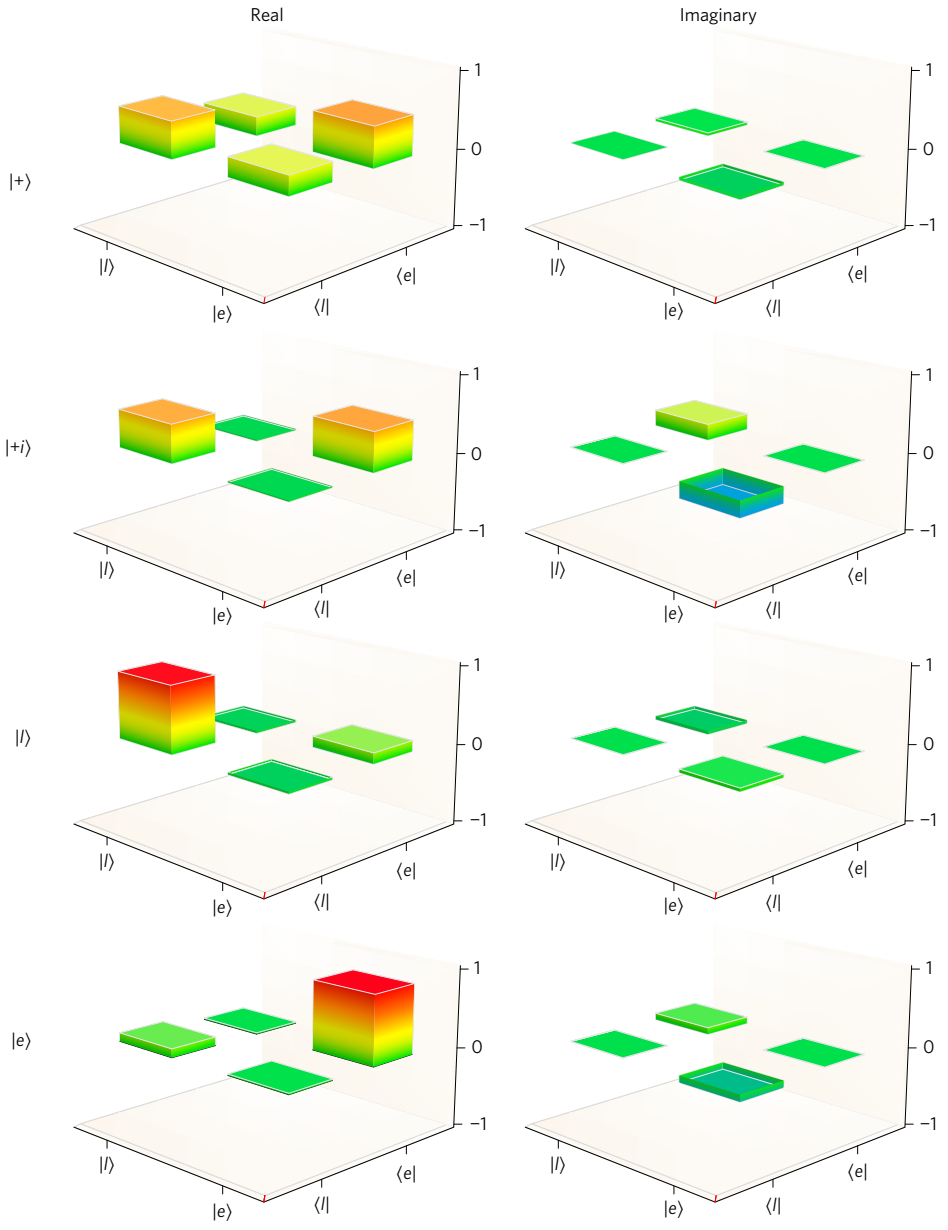

Figure 4 | Density matrices of four states after teleportation. Shown are the real and imaginary parts of the reconstructed density matrices for four different input states created at Alice. The mean photon number per qubit is $\mu_A = 0.014$ and the mean photon pair number is $\mu_{SPDC} = 0.045$. The state labels denote the states expected after teleportation.

remaining distinguishability of the two photons subjected to the BSM at Charlie, followed by multi-pair emissions by the pair source. Finally, by averaging the single-photon fidelities over all input states, weighted as above, we find $\langle F^{(1)} \rangle \geq (80 \pm 2)\%$, as before significantly violating the threshold between classical and quantum teleportation.

Our measurements establish the possibility for quantum teleportation over many kilometres in the important mid-point configuration, as is required for extending the distance of quantum communications using quantum repeaters. We emphasize that both photons travelling to Charlie are at a telecommunication wavelength, making it possible to extend the Alice–Bob distance from its current value of 8 km by at least one order of magnitude. This corresponds to the distance of an elementary link, which includes teleportation of entanglement, at which communication links based on spectrally multiplexed quantum repeaters start to outperform direct qubit transmission[21,22].

We also note that the 795 nm photon, both in terms of central wavelength and spectral width, is compatible with quantum memory for light (a key element of a quantum repeater) in cryogenically cooled thulium-doped crystals[23]. This, in conjunction with projection onto two Bell states[24], would allow us to implement active feedforward on the teleported photon. An interesting question is whether our implementation—in particular the laser used to stabilize the phase in Alice's and Bob's interferometers—opens side channels for eavesdropping. While this topic is beyond the scope of our investigation, we emphasize that lasers with sufficient stability to allow for local (independent) stabilization are available[25].

Finally, we point out that quantum teleportation involves the interesting aspect of Alice transferring her quantum state in a disembodied fashion to Bob without him ever receiving any physical particle. In other words, Bob is only sending photons (all of them members of an entangled pair) and thus is better able to

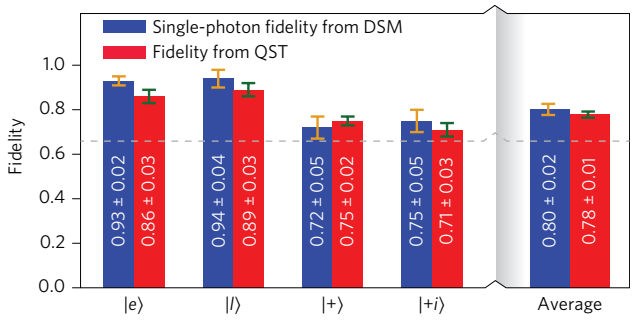

Figure 5 | Individual and average fidelities of four teleported states with expected (ideal) states, measured using quantum state tomography (QST) and the decoy-state method (DSM). For the DSM we set $\mu_{SPDC} = 0.06$. Error bars (one standard deviation) are calculated assuming Poissonian detection statistics and using Monte Carlo simulation. Count rates for both methods are provided in Supplementary Section 7. The larger degradation of $|+\rangle$ and $|+i\rangle$ states is due to the limited quality of the BSM (Supplementary Section 5) and imperfect interferometers. Neither cause an effect for $|e\rangle$ and $|l\rangle$ states.

protect his system from any outside interference, for example, from an adversary[26].

We note that a related experimental demonstration has been reported in a concurrent manuscript[27].

Methods

Methods and any associated references are available in the online version of the paper.

Received 11 March 2016; accepted 9 August 2016; published online 19 September 2016

References

1. Bennett, C. H. *et al.* Teleporting an unknown quantum state via dual classical and Einstein–Podolsky–Rosen channels. *Phys. Rev. Lett.* **70,** 1895–1899 (1993).
2. Pirandola, S., Eisert, J., Weedbrook, C., Furusawa, A. & Braunstein, S. L. Advances in quantum teleportation. *Nat. Photon.* **9,** 641–652 (2015).
3. Landry, O., van Houwelingen, J. A. W., Beveratos, A., Zbinden, H. & Gisin, N. Quantum teleportation over the Swisscom telecommunication network. *J. Opt. Soc. Am. B* **24,** 398–403 (2007).
4. Hensen, B. *et al.* Loophole-free Bell inequality violation using electron spins separated by 1.3 kilometres. *Nature* **526,** 682–686 (2015).
5. Sangouard, N., Simon, C., De Riedmatten, H. & Gisin, N. Quantum repeaters based on atomic ensembles and linear optics. *Rev. Mod. Phys.* **83,** 33–80 (2011).
6. Kimble, H. J. The quantum internet. *Nature* **453,** 1023–1030 (2008).
7. Yin, J. *et al.* Quantum teleportation and entanglement distribution over 100-kilometre free-space channels. *Nature* **488,** 185–188 (2012).
8. Ma, X.-S. *et al.* Quantum teleportation over 143 kilometres using active feed-forward. *Nature* **489,** 269–273 (2012).
9. Lvovsky, A. I., Sanders, B. C. & Tittel, W. Optical quantum memory. *Nat. Photon.* **3,** 706–714 (2009).
10. Żukowski, M., Zeilinger, A., Horne, M. A. & Ekert, A. K. 'Event-ready-detectors' Bell experiment via entanglement swapping. *Phys. Rev. Lett.* **71,** 4287–4290 (1993).
11. Rubenok, A., Slater, J. A., Chan, P., Lucio-Martinez, I. & Tittel, W. Real-world two-photon interference and proof-of-principle quantum key distribution immune to detector attacks. *Phys. Rev. Lett.* **111,** 130501 (2013).
12. Marcikic, I., De Riedmatten, H., Tittel, W., Zbinden, H. & Gisin, N. Long-distance teleportation of qubits at telecommunication wavelengths. *Nature* **421,** 509–513 (2003).
13. de Riedmatten, H. *et al.* Long distance quantum teleportation in a quantum relay configuration. *Phys. Rev. Lett.* **92,** 047904 (2004).
14. Bussières, F. *et al.* Quantum teleportation from a telecom-wavelength photon to a solid-state quantum memory. *Nat. Photon.* **8,** 775–778 (2014).
15. Takesue, H. *et al.* Quantum teleportation over 100 km of fiber using highly efficient superconducting nanowire single-photon detectors. *Optica* **2,** 832–835 (2015).
16. Ma, X. S. *et al.* Experimental delayed-choice entanglement swapping. *Nat. Phys.* **8,** 479–484 (2012).
17. Megidish, E. *et al.* Entanglement swapping between photons that have never coexisted. *Phys. Rev. Lett.* **110,** 210403 (2013).
18. Massar, S. & Popescu, S. Optimal extraction of information from finite quantum ensembles. *Phys. Rev. Lett.* **74,** 1259–1263 (1995).
19. Lo, H.-K., Ma, X. & Chen, K. Decoy state quantum key distribution. *Phys. Rev. Lett.* **94,** 230504 (2005).
20. Wang, X. B. Beating the photon-number-splitting attack in practical quantum cryptography. *Phys. Rev. Lett.* **94,** 230503 (2005).
21. Sinclair, N. *et al.* Spectral multiplexing for scalable quantum photonics using an atomic frequency comb quantum memory and feed-forward control. *Phys. Rev. Lett.* **113,** 053603 (2014).
22. Krovi, H. *et al.* Practical quantum repeaters with parametric down-conversion sources. *Appl. Phys. B* **122,** 52 (2016).
23. Thiel, C. W., Sinclair, N., Tittel, W. & Cone, R. L. Optical decoherence studies of Tm^{3+} : $Y_3Ga_5O_{12}$. *Phys. Rev. B* **90,** 214301 (2014).
24. Valivarthi, R. *et al.* Efficient Bell state analyzer for time-bin qubits with fast-recovery WSi superconducting single photon detectors. *Opt. Express* **22,** 24497–24506 (2014).
25. Wavelength References *Data Sheets and Pkg Drawings*; http://www.wavelengthreferences.com/pdf/Data
26. Braunstein, S. L. & Pirandola, S. Side-channel-free quantum key distribution. *Phys. Rev. Lett.* **108,** 130502 (2012).
27. Sun, Q.-C. *et al.* Quantum teleportation with independent sources and prior entanglement distribution over a network. *Nat. Photon.* http://dx.doi.org/10.1038/nphoton.2016.179 (2016).
28. Brendel, J., Gisin, N., Tittel, W. & Zbinden, H. Pulsed energy-time entangled twin-photon source for quantum communication. *Phys. Rev. Lett.* **82,** 2594–2597 (1999).
29. Marsili, F. *et al.* Detecting single infrared photons with 93% system efficiency. *Nat. Photon.* **7,** 210–214 (2013).
30. Hong, C. K., Ou, Z. Y. & Mandel, L. Measurement of subpicosecond time intervals between two photons by interference. *Phys. Rev. Lett.* **59,** 2044–2046 (1987).

Acknowledgements

The authors thank T. Andruschak, R. Angelo, D. Basto, C. Chambers and H. Dhillon from the City of Calgary for providing access to the fibre network and for help during the experiment, V. Kiselyov for technical support and P. Lefebvre for help with aligning the entangled photon pair source. This work was funded through Alberta Innovates Technology Futures (AITF), the National Science and Engineering Research Council of Canada (NSERC) and the Defense Advanced Research Projects Agency (DARPA) Quiness programme (contract no. W31P4Q-13-1-0004). W.T. also acknowledges funding as a Senior Fellow of the Canadian Institute for Advanced Research (CIFAR), and V.B.V. and S.W.N. acknowledge partial funding for detector development from the Defense Advanced Research Projects Agency (DARPA) Information in a Photon (InPho) programme. Part of the detector research was carried out at the Jet Propulsion Laboratory, California Institute of Technology, under a contract with the National Aeronautics and Space Administration.

Author contributions

The SNSPDs were fabricated and tested by V.B.V., F.M., M.D.S. and S.W.N. The experiment was conceived and guided by W.T. The set-up was developed, measurements were performed, and the data were analysed by R.V., M.G.P., Q.Z., G.H.A. and D.O. The manuscript was written by W.T., R.V., M.G.P., Q.Z., G.H.A. and D.O.

Additional information

Supplementary information is available in the online version of the paper. Reprints and permissions information is available online at www.nature.com/reprints. Correspondence and requests for materials should be addressed to W.T.

Competing financial interests

The authors declare no competing financial interests.

Methods

Synchronization. For the following discussion, see the experimental set-up outlined in Fig. 2. Charlie is connected via pairs of optical fibres to both Alice and Bob. In each pair, one fibre (referred to as the quantum channel, QC) carries photonic qubits, while the other (referred to as the classical channel, CC) distributes various strong optical signals whose purpose will be described in the following. In addition, Alice and Bob are directly connected via an optical fibre that transmits narrow-linewidth laser light at 1,550 nm in order to lock the phases of all interferometers (that is, γ, ξ and θ, as shown in Fig. 2). This is crucial for maintaining a common phase reference for the qubit states generated at Alice and Bob, and analysed at Bob. In each interferometer, the power of the locking laser in one output arm (measured on a classical detector) is used to derive a feedback signal to a piezo-element that regulates the path-length difference of the interferometer to maintain a fixed phase. For instance, for free-space-optics-based interferometers at Bob, the path-length difference is changed by moving a mirror with the piezo stack, while for the fibre-optics interferometer at Alice, the path-length is adjusted by stretching a fibre wrapped around a piezo-tube. Additionally, all interferometers are kept in temperature-controlled boxes.

The master clock for all devices is derived from detection of the mode-locked laser pulses (80 MHz) and converted back into an optical signal for distribution through the CC via Charlie to Alice.

Stabilization to ensure photon indistinguishability. For a successful BSM, the photons arriving at Charlie from Alice and Bob need to be indistinguishable, despite being generated by independent and different sources, and having travelled through several kilometres of deployed fibre. The spatial indistinguishability is naturally ensured by the propagation in single-mode optical fibres. To ensure that the photons have the same spectral profile, they are sent through separate, temperature-stabilized fibre Bragg gratings (FBGs) that narrow their spectra to 6 GHz. The spectral overlap of the FBGs at Alice and Bob needs to be set only once. However, due to the temperature-dependent properties of fibre, such as birefringence and length, the polarization and arrival time of the photons change with external environmental conditions, making it difficult to implement the BSM in a real-world environment. Towards this end, we apply feedback mechanisms to compensate for drifts in polarization and arrival time.

Timing. The short duration of our photons (70 ps) prevents us from using the superconducting nanowire single-photon detectors (SNSPDs) (featuring a time jitter of ~150 ps) to directly determine their arrival times with the required precision to adjust the difference to zero. Instead, we compensate for arrival-time drifts with the novel approach of observing the degree of quantum interference (the Hong–Ou–Mandel (or HOM) effect[30]) of the photons. The signals from the two SNSPDs (which are used to perform the BSM) are also sent to a HOM analysing unit (Fig. 2) that monitors the number of coincidences between detections corresponding to either both photons arriving in an early time bin mode, or both in a late bin. As shown in the inset of Fig. 3b, the HOM interference causes photon bunching and thus the coincidences to be reduced when the photons arrive at the beamsplitter at the same time. Hence, to counteract the drift in the travel time of the photons, we vary the qubit generation time at Alice with a precision of ~4 ps to keep the coincidence count rate at the minimum value of ~750 per 10 s, as shown in Fig. 3b. In practice, Alice's time shift is triggered at Charlie by shifting the phase of the master clock signal that he forwards to Alice. Figure 3b shows that, during a typical 1.5 h measurement, we apply a time shift of ~200 ps to compensate drifts in timing. Because the shift is larger than the duration of the photons, the teleportation protocol would fail without the active stabilization.

Polarization. Because photons from Alice and Bob pass through polarizing beamsplitters (PBS) at Charlie, their polarization indistinguishability is naturally satisfied. However, correct photon polarizations must be set and maintained to maximize the transmission through the PBSs, or the channel loss will vary over time. In our system, the QC between Bob and Charlie experiences only a slow drift, which allows for manual compensation using a polarization controller—located at Bob—once a day. However, an automated polarization feedback system is required for the channel between Alice and Charlie, which drifts significantly on the timescale of the experiment. To that end, we monitor the count rate of an additional SNSPD, located in the reflection port of the PBS at Charlie, with a field-programmable gate-array (FPGA) so as to generate a feedback signal that minimizes the rate by adjusting the polarization by means of a polarization tracker (also located at Charlie). As seen in Fig. 3, the intensity fluctuations in 1.5 h (a typical timescale to acquire results for one qubit setting) are limited to 5% with feedback, and to about 15% without feedback.

Data collection. Using Alice's qubits and the 1,532 nm members of the entangled pairs, Charlie performs $|\psi^-\rangle$ Bell-state projections. Such a projection occurs when one SNSPD detects a photon arriving in the early time bin and the other SNSPD records a photon in the late time bin. Successful Bell-state projection measurements are communicated via the CC and using classical laser pulses to Bob, who converts them back to electrical signals. Each signal is then used to form a triple coincidence with the detection signal of the 795 nm wavelength photon exiting Bob's qubit analyser. Towards this end, the latter is delayed using a variable electronic delay line (VEDL) implemented on an FPGA by the time it takes the 1,532 nm entangled photon to travel from Bob to Charlie plus the travel time of the BSM signal back to Bob.